

Activation Quantization of Vision Encoders Needs Prefixing Registers

Seunghyeon Kim¹, Taesun Yeom¹, Jinho Kim², Wonpyo Park³, Kyuyeun Kim³, Jaeho Lee^{1*}
 POSTECH¹, Dankook University², Google³

{shkim0418, tsyeom, jaeho.lee}@postech.ac.kr, sunder990@dankook.ac.kr
 {wppark, kyuyeunk}@google.com

Abstract

Large pretrained vision encoders are central to multimodal intelligence, powering applications from on-device vision processing to vision-language models. Since these applications often demand real-time processing of massive visual data, reducing the inference cost of vision encoders is critical. Quantization offers a practical path, but it remains challenging even at 8-bit precision due to so-called outliers. In this work, we propose *RegCache*, a training-free algorithm that mitigates outliers in large-scale pretrained vision encoders and serves as a plug-in module that can be applied on top of other quantization methods. *RegCache* introduces outlier-prone yet semantically meaningless prefix tokens to the vision encoder, which prevent other tokens from having outliers. Notably, we observe that outliers in vision encoders behave differently from those in language models, motivating two technical innovations: middle-layer prefixing and token deletion. Experimental results show that our method consistently improves quantized model performance across various vision encoders, particularly in extremely low-bit regimes (e.g., 4-bit).

1. Introduction

Transformer-based vision encoders, such as CLIP and DINOv2, lie at the core of modern multimodal systems [41, 43]. Leveraging the scalability of vision transformers (ViTs) [14], these models are pretrained on massive datasets using large-scale computation, yielding highly informative and versatile visual representations. However, their large size poses challenges for practical deployment. Vision encoders are frequently deployed as standalone models on edge devices, where storage limits and inference overhead become major bottlenecks [16].¹ Vision encoders also serve as the visual backbones of many vision-language models (VLMs)

*Corresponding Author.

¹To this end, several vendors provide deployment-ready lightweight vision encoders and toolchains for edge processors; see, e.g., NVIDIA (NV-CLIP), Qualcomm AI Hub (OpenAI CLIP), and Hailo (Hailo-CLIP).

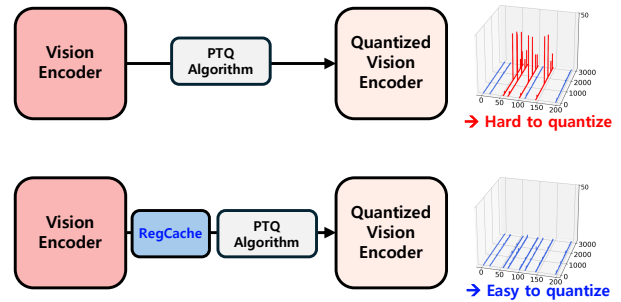


Figure 1. A diagram of the proposed *RegCache* framework, pre-processing the vision encoder before PTQ.

[3, 31], where their computational cost remains substantial, especially for high-resolution images or video [27, 50]. In video pipelines, the vision encoder can account for roughly 45% of overall latency, and may even exceed the LLM pre-filling cost at high resolutions [27, 50].

To address these challenges, post-training quantization (PTQ) offers a practical solution, reducing memory usage and computational cost without additional training [9]. However, despite recent progress, PTQ methods for ViT-based vision encoders still suffer from significant performance degradation under low-bit quantization [28, 51, 59]. Moreover, unlike autoregressive large language models (LLMs), which are often memory-bound on GPU servers, vision encoders are typically non-autoregressive and thus more likely to operate in compute-bound regimes.² Quantizing both activations and weights therefore allows high-precision matrix multiplications to be replaced with low-precision operations (e.g., INT8), hence reducing computational cost.

However, activation quantization of large pretrained transformers is challenging due to *outlier* activations—i.e., a small number of extremely large activations that often

²In contrast, the memory-bound nature of autoregressive LLM inference running on GPU servers renders weight-only quantization to be particularly effective.

arise in a few channels of later layers [46]. These outliers significantly expand the activation quantization range, leading to large quantization errors. While outlier-robust quantization has been widely studied for LLMs [13, 29, 52], existing methods typically assign different precision levels or quantization ranges to individual tokens or channels. This introduces substantial overhead, making them difficult to apply in static activation quantization settings [7, 45].

An emerging alternative is to directly mitigate outliers by prefixing *attention sink* tokens—i.e., semantically meaningless tokens such as $\langle \text{BOS} \rangle$ or $\langle \text{SEP} \rangle$ that absorb large attention from other tokens [46, 53]. Recent studies on LLM quantization show that inserting the activations of these sink tokens as a prefix in each attention layer can dramatically reduce the activation magnitudes of other tokens, thereby improving PTQ performance [7, 45, 55].

Naturally, one may ask: *Can we mitigate outliers in vision encoders by prefixing attention sinks?* Unfortunately, it remains unclear which token in a vision encoder (i.e., a patch embedding) could play a role analogous to attention sinks in language models. Unlike LLMs, typical vision encoders are not pretrained with tokens that are explicitly designed to be semantically meaningless (Fig. 2). Recent work suggests that introducing such meaningless tokens—termed *registers*—during training can improve the interpretability of ViT-based models [11]. However, incorporating registers remains uncommon in vision encoders.³

Contribution. In this work, we introduce *RegCache* (Register Caching), a novel prefix-based outlier mitigation algorithm for quantizing pretrained vision encoders. RegCache is inspired by the following empirical observation:

Sink tokens emerge gradually from the **middle** layers of vision encoders, giving rise to outliers. These tokens are **highly similar across images**, enabling their use as a **universal register** for any input at test time.

Based on these observations, which distinguish large pretrained vision encoders from relatively small ViTs, RegCache mitigates outliers by discovering and prefixing middle-layer registers to the vision encoder in the form of a precomputed key-value (KV) cache. Notably, unlike in LLM prefixing [45], these tokens are inserted only in the middle-to-final layers and do not affect the early layers. RegCache also removes the remaining sink tokens that exhibit unusually large outliers. Through this process of adding and deleting tokens, RegCache replaces internally emerging sink tokens with external precomputed caches, preventing them from inflating the activation quantization

range. Importantly, this procedure requires no additional training of the vision encoder, rendering RegCache a versatile go-to method. In practice, RegCache can be integrated as a lightweight on-top module into existing PTQ pipelines.

Throughout experiments, we apply RegCache to diverse text- and self-supervised vision encoders and combine it with recent PTQ methods for ViTs, which can be further improved by mitigating large activation outliers. We observe that such combinations consistently improve the prediction accuracy of quantized vision encoders across all considered setups. Notably, these gains are most pronounced under extremely low-bit quantization (e.g., 4-bit).

2. Related work

Outliers in large-scale transformers. In large-scale transformers, some activations in certain layers can attain magnitudes significantly larger than others—a phenomenon known as the *emergence of outliers* [5, 13, 25, 48]. Sun et al. [46] provide a systematic analysis and show that these outliers arise from the softmax operation in self-attention in both LLMs and ViTs. In LLMs, extreme activations are often concentrated on special tokens such as $\langle \text{BOS} \rangle$ or $\langle \text{SEP} \rangle$. In ViTs, several studies report that outlier tokens typically correspond to uninformative background patches, and removing them can improve internal representations [11, 23, 37]. However, it remains unclear which specific visual tokens consistently produce outliers in ViT-based vision encoders, as the corresponding patches vary across images. To address this gap, we observe that outlier tokens typically emerge in intermediate blocks and exhibit similar features across images and across a wide range of vision encoders, enabling them to be precomputed for downstream use cases such as PTQ.

Improving vision transformers via controlling attention sink tokens.

Attention sinks, first highlighted by Xiao et al. [53], are tokens with little or no semantic content that nonetheless attract excessive attention in both LLMs [21] and ViTs [11]. In ViTs, these sink tokens act as noise in the attention map, hindering the model’s ability to capture relations between patches and degrading downstream visual performance [11, 23, 24, 37]. To mitigate this issue, Darcet et al. [11] introduce an additional register token during training to absorb attention sinks that emerge in image patches. More recently, Jiang et al. [23] propose a training-free *test-time register* that relocates the maximum activations from channels that frequently exhibit outliers into an extra token during inference. From a different perspective, we instead leverage sink tokens to suppress outliers that degrade PTQ performance. Our method employs an external, precomputed sink token, enabling efficient inference without per-image processing while reducing the activation dynamic range prior to quantization.

³In this regard, DINOv3 is a pleasant exception [44].

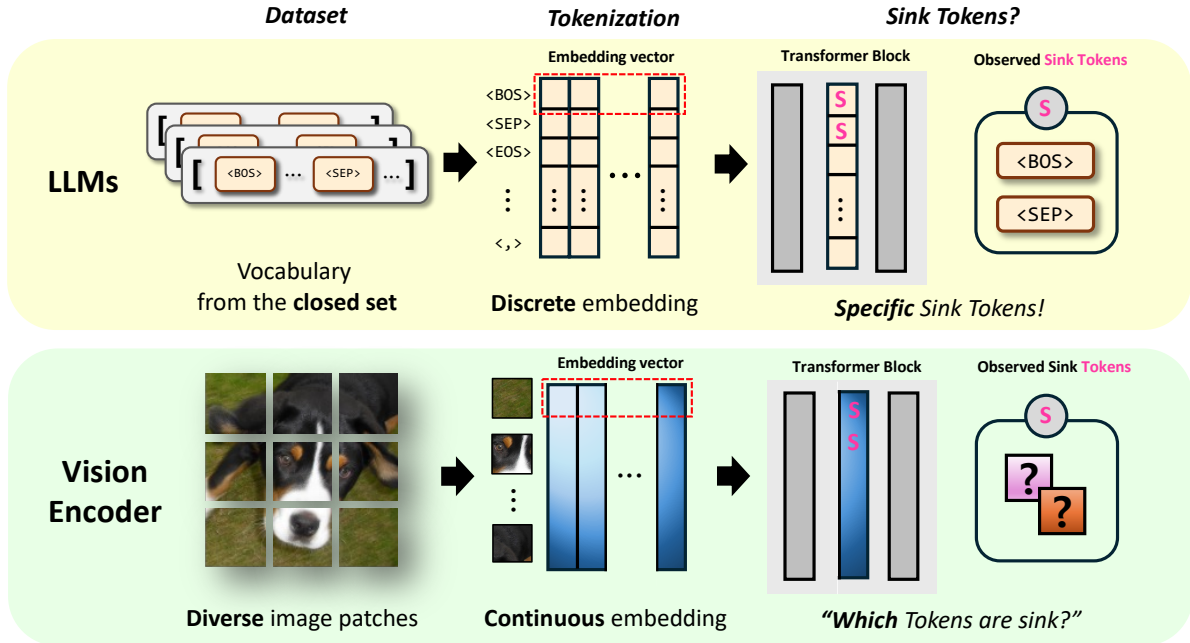


Figure 2. **Sink tokens in LLMs vs. vision encoders.** Unlike LLMs, where sink tokens exist in a closed-set vocabulary, vision encoders process diverse image patches continuously mapped into an embedding space, making sink token discovery more challenging.

Post-training quantization for vision transformers.

Prior work has explored reducing the inference cost of large-scale ViT-based models through PTQ. Early methods mitigate quantization errors by assigning dynamic bitwidths to self-attention-sensitive blocks [35]. Subsequent studies attribute the low PTQ performance of ViTs to activation outliers arising from operations such as LayerNorm, softmax, and GELU. Motivated by this observation, RepQ-ViT [28] and PTQ4ViT [56] propose quantization schemes that isolate and minimize the impact of outliers. Other approaches address the heavy-tailed activation distribution; for example, NoisyQuant [34] injects noise to reshape the activation distribution. FIMA-Q [51] introduces round-function optimization for PTQ, while ERQ [59] proposes a two-step procedure that sequentially quantizes activations and weights to reduce quantization error.

Outlier control strategy in quantization. Majority of PTQ methods reduce quantization error by employing specialized quantizers for heavy-tailed activations [56, 59], scale reparameterization [28, 59], distribution reshaping [34], quantizer optimization [51], and ridge regression [59]. While these methods are applied in the presence of outliers, RegCache directly suppresses outliers by leveraging a structural property of the vision encoder. Thus, RegCache can be easily integrated into existing PTQ pipelines to further reduce quantization error.

3. A closer look at outliers in vision encoders

Outliers in vision encoders tend to emerge at seemingly random background patch tokens for a given image, whereas in LLMs they typically occur at specific token positions or types [11, 46]. This lack of consistency makes it difficult to mitigate outliers in vision encoders through prefixing [45], as such strategies require caching tokens that universally induce outliers across arbitrary test-time inputs (i.e., registers).

In this section, we present three key findings that motivate an alternative strategy—*identifying universal sink tokens in the middle blocks of the model and prefixing them there*. These findings also shed light on why outliers in vision encoders predominantly emerge in the middle layers.

- Section 3.1: Quantization-sensitive layers primarily occur in the middle of the network, where outliers emerge, while remaining low elsewhere; thus, prefixing is unnecessary in early layers.
- Section 3.2: We explain why outliers emerge later in the network: early layers first identify semantically meaningful tokens.
- Section 3.3: In the middle layers, outlier tokens become highly similar across images, suggesting that they act as universal registers.

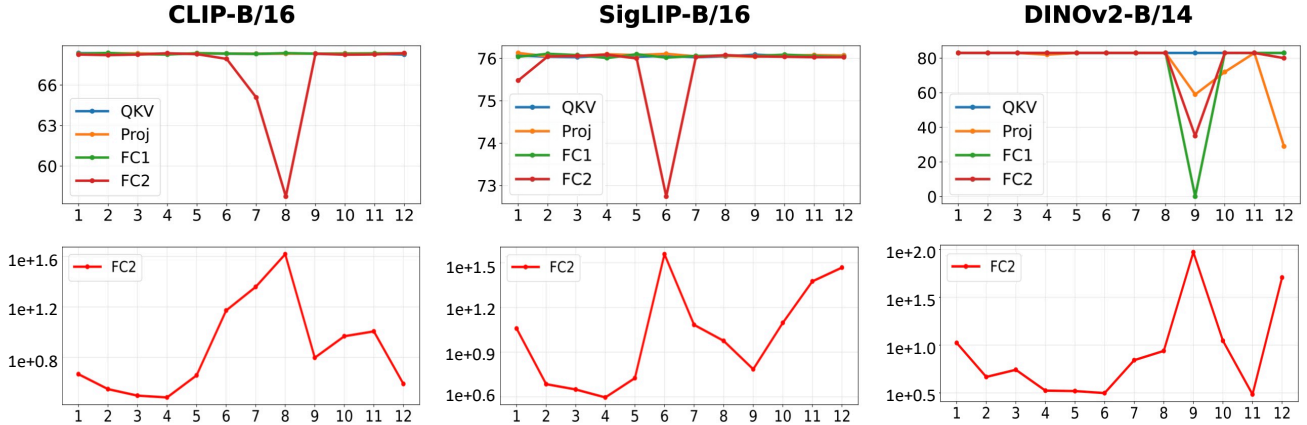


Figure 3. **(Top) Layerwise quantization sensitivity (%)**. We plot the zero-shot ImageNet-1k accuracy when quantizing each layer individually to W8A8. **(Bottom) Maximum norm of the FC2 layer input tokens for each layer**. We plot the largest ℓ_∞ -norm across all tokens per image on a log scale, averaged over the ImageNet-1k validation set. For both plots, the x-axis denotes the transformer block index.

3.1. Layerwise quantization sensitivity and outliers

We first analyze the quantization sensitivity of each layer in vision encoders and examine its connection to the emergence of activation outliers (i.e., FC2 inputs). In Fig. 3 (top), we report the layerwise quantization sensitivity, measured as the zero-shot ImageNet-1k accuracy when a given layer is quantized to W8A8. We observe that quantization-sensitive layers—i.e., layers that incur substantial accuracy drops when quantized—are highly localized to the MLP projection layers in one or two middle layers. In DINOv2, the performance degradation is particularly pronounced, and takes place in other layers as well. Moreover, as shown in Fig. 3 (bottom), these quantization-sensitive layers coincide with the blocks where activation outliers in the hidden states begin to emerge. Together, these results suggest that outliers are a primary driver of performance degradation when quantizing vision encoders. In Sec. I, we further analyze the effect of outlier tokens under quantization, highlighting the importance of mitigating them to improve PTQ performance.

In particular, we establish a clear connection between quantized accuracy and the high-norm activation behavior. Our findings further suggest that monitoring FC2 activations or directly measuring quantization sensitivity can help identify the blocks where prefixing should be applied. Additional results for other vision encoders (OpenCLIP and SigLIP2) are provided in Sec. A.

3.2. Why the middle layers?

A natural question arises: Why do outliers in vision encoders emerge in the middle layers, whereas in LLMs they appear in the early layers? We hypothesize that this differ-

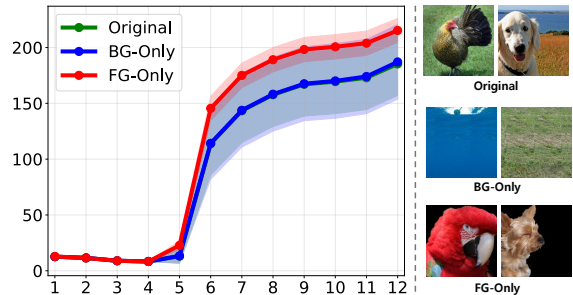


Figure 4. **Outliers in FG/BG-only images, for SigLIP-B/16 model**. Note that “Original” and “BG-only” nearly overlaps.

ence stems from the difficulty of identifying *semantically meaningless* tokens from raw image patches. Such tokens become distinguishable only after several processing blocks of the vision encoder. In contrast, in LLMs some tokens are clearly meaningless from the outset, such as $\langle \text{BOS} \rangle$, $\langle \text{SEP} \rangle$ (see Fig. 2, left).

To test this hypothesis, we design an experiment that compares the emergence of outliers in images where meaningless patches are easily identifiable against those where the distinction is less clear. Specifically, using the test set of ImageNet-9 [54], we compare foreground-only images—where the background pixels are zero-ed out—with the original images. In foreground-only images, semantically meaningless patches should be easier to identify, requiring fewer processing blocks.

As shown in Fig. 4, outliers in foreground-only images emerge earlier and with larger magnitude than in the original images, supporting our hypothesis. In contrast, removing the foreground and retaining only the background leaves the outlier behavior largely unchanged (i.e., the curves

nearly overlap). In Sec. M, we further analyze vision encoders trained with registers, where meaningless tokens are explicitly defined. These models exhibit behavior similar to LLMs, with outliers emerging from the early layers.

3.3. Universality of outlier tokens

Next, we examine the outlier tokens in the quantization-sensitive layer. Specifically, we measure the cosine similarity between middle-layer FC2 input outlier tokens (i.e., those with the largest ℓ_∞ -norm) extracted from pairs of images. Using 64 randomly sampled images from the ImageNet-1k validation split, we compute the mean pairwise cosine similarity.

From Tab. 1, outlier tokens are highly similar across images, with a mean cosine similarity of 0.89. In contrast, normal tokens are much less similar, with an average of only 0.26. This suggests that outliers contain components largely independent of the input image and may represent universal features that persist across samples. In Sec. F, we provide a theoretical explanation for this phenomenon, showing that it arises from the large magnitude of the outliers and the alignment of their locations (i.e., channels).

4. Method

Before introducing our method, we recall two observations from the Sec. 3:

- In vision encoders, outliers tend to emerge in the middle layers (e.g., fully-connected layers in blocks 5–8), whereas in LLMs they begin to appear in the early layers.
- Sink tokens (i.e., outlier-prone tokens) discovered in the middle layers are highly similar across images.

Combining these observations with prior findings in LLMs—prefixing additional sink tokens can mitigate outliers [45]—we arrive at the following hypothesis:

“Middle-layer sink tokens from one image can act as registers and help mitigate outliers in vision encoders processing another image.”

Based on this hypothesis, we propose RegCache (Register Caching), an outlier-mitigation algorithm that replaces internally emerging sink tokens by inserting register tokens discovered from reference images. In essence, RegCache operates in three steps (see Fig. 5).

- (1) **Curating** a set of register candidate tokens—i.e., with large activation magnitudes—from a pool of reference images. ▷ Sec. 4.1
- (2) **Caching** the keys and values of selected register candidates to the sensitive layers. ▷ Sec. 4.2

- (3) **Deleting** internally emerging sink tokens to clean up remaining outliers. ▷ Sec. 4.3

RegCache requires no additional training and only performs several rounds of validation on a reference task and dataset, as will be discussed below. As a result, the algorithm does not require large amounts of data or substantial computational resources. At inference time, RegCache temporarily adds and removes a few tokens, introducing only negligible overhead (see Sec. 5.4).

4.1. Curating

Given a pretrained vision encoder, we first identify the quantization-sensitive layer of the model. We then construct a curated set of register candidate tokens by selecting the top- k tokens with the largest activation in this layer from a pool of reference images.

Identifying the quantization-sensitive layer. Following Sec. 3.1, we quantize each layer of the vision encoder independently, and select the one that yields the largest accuracy drop on a reference task as the quantization-sensitive layer. If a specific base quantization algorithm is intended for deployment, we use it during this analysis; otherwise, we use standard round-to-nearest quantization. As the reference task, we use ImageNet-1k classification (on the training split), which is widely regarded as representative of visual understanding. As a label-free alternative, we also provide a reconstruction-loss-based approach that leverages unlabeled data (see Sec. K).

Curating the set of register candidates. After identifying the quantization-sensitive layer, we construct a set of register candidate tokens likely to act as registers when inserted near this layer. Specifically, we run inference on a pool of reference images and select the tokens with the largest ℓ_∞ norm at the quantization-sensitive layer. Formally, let l_q denote the quantization-sensitive layer identified via the sensitivity analysis in Sec. 3.1, and let $\Phi_l(\mathbf{x})$ denote the set of tokens at the input of the l -th layer for an image \mathbf{x} . We construct the register candidate set as

$$\mathcal{S} = \operatorname{argtopk} \{ \|\mathbf{z}\|_\infty \mid \mathbf{z} \in \Phi_{l_q}(\mathbf{x}), \text{ for some } \mathbf{x} \in \mathcal{I}_{\text{ref}} \}, \quad (1)$$

where \mathcal{I}_{ref} denotes the pool of reference images. In our experiments, we sample 50,000 images from the ImageNet-1k training split and set $k = 100$. Since sink tokens often emerge several blocks before the quantization-sensitive layer, we perform the same search for up to three preceding blocks, constructing separate register candidate sets for each block.

4.2. Caching

Having the set of register candidates \mathcal{S} constructed, we compose the register by simply averaging the KV caches

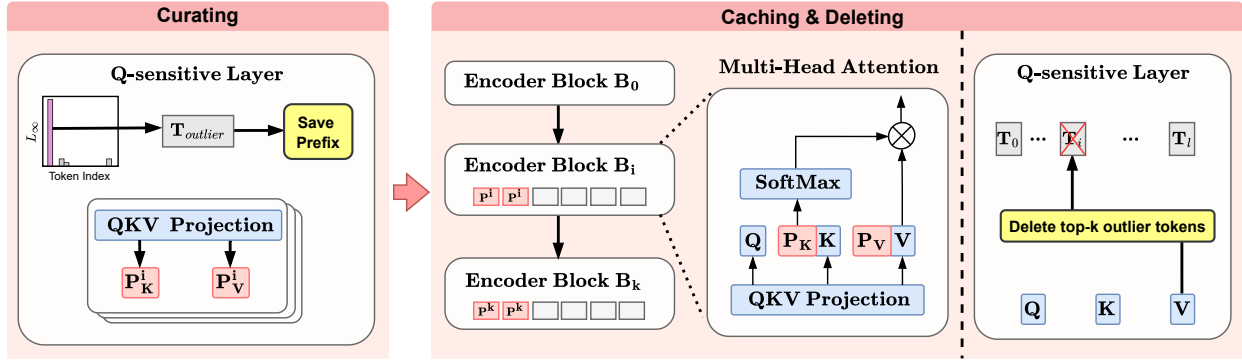


Figure 5. **An overview of the proposed RegCache algorithm.** We identify a universal register by analyzing the inputs of quantization-sensitive layers across blocks. During inference, the register is inserted into each block, and outlier tokens are removed from the most quantization-sensitive layer.

of the register candidate tokens $\mathbf{z}^* \in \mathcal{S}$. We then search for the optimal $\tau^* \in \mathbb{N}$, the number of times the register is copied and inserted into the target vision encoder. Precisely, the search is done as follows.

- First, we compute KV caches for each register candidate token $\mathbf{z} \in \mathcal{S}$, for blocks starting from the few layers before the quantization-sensitive block, as well as all subsequent blocks using the *unquantized* vision encoder.
- Then, we insert the averaged KV cache to the *quantized* vision encoder, with different number of copies. We vary τ within the range $\{1, 2, \dots, 15\}$ and select τ^* the one with the highest reference task accuracy.⁴ Here, as in Sec. 4.1, we consider classification on the training split of ImageNet-1k dataset as our reference task.

4.3. Deleting

Finally, we apply a *token deletion* process to the input of the quantization-sensitive block (i.e., the block where l_q is located) in the vision encoder. At the inference phase, this process removes the sink tokens that emerge among the image patch tokens, thus removing any remaining outliers. Precisely, given some test image \mathbf{x}_{test} , we select the tokens with the top- \tilde{k} ℓ_∞ norm, i.e.,

$$\mathcal{D} = \text{argtop}_{\tilde{k}} \{ \|\mathbf{z}\|_\infty \mid \mathbf{z} \in \Phi_{l_q}(\mathbf{x}_{\text{test}}) \} \quad (2)$$

and remove these tokens from the model. Here, similarly to the curating and caching steps, the number of tokens to be removed—i.e., \tilde{k} —is tuned using the reference task.

5. Experiments

In this section, we first describe our experimental setup in Sec. 5.1. Next, we report results for both standalone vision

⁴The total search cost of our algorithm is about 1 hour when using a naïve RTN pseudo-quantization algorithm on an RTX 4090.

encoders and VLMs across various benchmarks in Sec. 5.2, demonstrating consistent gains from RegCache over baselines. We also assess the generalizability of the pre-computed prefix tokens and further validate our design through analyses of prefix-token behavior, ablation studies, and latency measurements.

5.1. Setup

Standalone vision encoders. We evaluate the proposed method on five widely used vision encoders: (1) CLIP [43], (2) OpenCLIP [8], (3) SigLIP [57], (4) SigLIP2 [49], and (5) DINOv2 [41], which cover a diverse training configurations. For evaluation, we measure the quality of the quantized vision encoders using zero-shot accuracy on two downstream tasks: (1) Image classification on ImageNet-1k [12] and (2) text-image retrieval on MS-COCO [30]. To further validate the generalizability of the prefix searched from ImageNet-1k, we evaluate on diverse classification benchmarks, including Stanford Cars [26], Flowers-102 [38], Food-101 [6], CIFAR-100, Caltech101 [17], Oxford-IIIT Pet [42], and DTD [10].

Vision-language models. We primarily use Qwen3-VL [2] (2B and 8B) as a strong, widely adopted open-source VLM that can handle both image and video modalities. Furthermore, to demonstrate the broad applicability of our method, we also evaluate it on other VLMs, such as LLaVA [31] (see Sec. D for the results).

We evaluate image understanding on GQA [22] and VQAv2 [19], as visual question-answering benchmarks. For video understanding, we use Video-MME [18] to assess multi-domain reasoning and MLVU [61], which includes long-video evaluation where vision-encoder overhead can become a critical bottleneck.

Table 2. **Zero-shot classification accuracy on ImageNet-1k.** We have used various base quantization algorithms to quantize to 4/6/8 bits. The best results are marked in **bold**. Best/Average Δ denote the maximum/average accuracy gaps between each baseline and its RegCache counterpart, excluding the Naïve cases.

Method	CLIP-B/16			OpenCLIP-B/16			SigLIP-B/16			SigLIP2-B/16			DINOv2-B/14		
	W4A4	W6A6	W8A8	W4A4	W6A6	W8A8	W4A4	W6A6	W8A8	W4A4	W6A6	W8A8	W4A4	W6A6	W8A8
FP32	68.32			70.22			76.05			78.47			83.26		
Naïve	0.09	0.17	34.01	0.10	0.47	46.12	0.13	0.77	69.71	0.14	0.19	26.04	0.00	0.01	19.20
w/ RegCache	0.07	0.44	59.71	0.10	1.20	66.90	0.10	24.41	74.38	0.11	0.26	72.35	0.18	0.42	22.34
PTQ4ViT	0.37	51.60	67.69	0.09	59.98	69.39	0.19	68.68	75.57	0.28	41.54	76.92	0.01	78.48	82.97
w/ RegCache	1.78	55.49	67.86	0.14	63.60	69.60	0.59	72.38	75.75	2.67	69.02	76.88	2.38	78.55	82.92
RepQ-ViT	1.83	53.25	67.39	1.18	46.51	68.70	21.36	73.32	75.23	0.40	64.91	76.43	4.52	19.61	82.27
w/ RegCache	21.50	66.73	68.10	11.10	68.22	70.06	33.76	74.52	75.94	10.15	75.40	77.13	4.97	22.38	81.55
NoisyQuant	0.34	46.19	63.20	2.50	59.05	67.08	1.78	71.10	75.50	0.46	44.50	70.83	1.61	49.25	71.46
w/ RegCache	1.42	57.41	65.82	10.41	67.51	69.36	9.19	72.28	75.64	0.54	62.60	76.44	2.04	48.65	70.38
FIMA-Q	50.41	66.51	67.63	60.09	67.24	68.53	76.05	76.06	76.06	78.48	78.47	78.48	OOM	OOM	OOM
w/ RegCache	62.08	66.70	67.86	65.11	68.62	69.13	76.13	76.12	76.12	78.38	78.37	78.37	OOM	OOM	OOM
ERQ	1.56	39.64	67.99	43.15	66.70	69.25	57.76	74.44	75.95	10.56	74.75	78.05	6.53	78.03	82.59
w/ RegCache	46.07	66.79	68.09	54.76	69.09	70.12	60.99	75.25	75.98	28.98	75.32	78.45	9.15	77.88	82.54
Best Δ	+44.51	+27.15	+2.62	+11.61	+21.84	+2.28	+12.40	+3.38	+0.71	+18.42	+27.48	+5.61	+2.62	+2.77	-0.05
Average Δ	+15.67	+11.19	+0.77	+6.90	+7.53	+1.06	+4.70	+1.35	+0.25	+6.11	+11.31	+1.36	1.11	+0.52	-0.47

Table 3. **Zero-shot image-text retrieval performance of CLIP and SigLIP on MS-COCO (R@1).** The results are reported in the same format as in Tab. 2.

	CLIP-B/16						SigLIP-B/16					
	Image \rightarrow Text			Text \rightarrow Image			Image \rightarrow Text			Text \rightarrow Image		
	W4A4	W6A6	W8A8	W4A4	W6A6	W8A8	W4A4	W6A6	W8A8	W4A4	W6A6	W8A8
FP32	52.94	52.94	52.94	32.73	32.73	32.73	67.68	67.68	67.68	47.19	47.19	47.19
Naïve	0.00	0.00	22.76	0.01	0.06	14.08	0.00	0.34	60.04	0.04	0.86	41.80
w/ RegCache	0.02	0.22	46.10	0.04	0.44	28.02	0.04	12.06	65.76	0.04	12.70	46.30
PTQ4ViT	0.06	37.28	52.78	0.17	23.00	32.00	0.20	60.66	66.86	0.78	41.73	47.16
w/ RegCache	0.52	43.46	53.54	0.14	26.51	32.48	2.10	61.42	67.72	1.78	43.05	47.61
RepQ-ViT	0.32	29.06	44.52	0.47	15.90	23.01	5.14	37.50	65.90	6.21	26.41	46.33
w/ RegCache	4.32	38.68	45.58	3.37	19.70	23.68	14.92	61.06	66.12	9.37	43.63	46.42
NoisyQuant	0.12	25.26	48.94	0.19	18.02	31.07	0.29	52.52	67.10	1.18	33.36	46.76
w/ RegCache	0.37	33.86	49.10	0.71	22.28	30.40	2.53	63.28	67.24	3.81	43.25	47.64
FIMA-Q	40.92	52.90	53.58	27.71	32.33	32.76	67.66	67.70	67.62	47.23	47.22	47.21
w/ RegCache	51.82	53.22	53.66	33.43	32.88	33.01	68.14	68.14	68.18	47.64	47.62	47.62
ERQ	0.32	23.62	44.78	3.71	15.58	23.31	28.96	61.94	65.80	20.70	43.48	46.46
w/ RegCache	13.78	40.88	44.86	6.52	19.82	23.52	32.66	62.30	66.16	23.21	44.61	46.63
Best Δ	+13.46	+17.26	+1.06	+5.72	+4.26	+0.67	+9.78	+23.56	+0.86	+5.41	+17.22	+0.88
Average Δ	+5.81	+8.40	+0.43	+2.19	+3.27	+0.19	+3.55	+7.18	+0.43	+3.10	+5.99	+0.40

Base quantization algorithms and details. To assess the broad applicability of RegCache as an effective on-top method, we evaluate it on four distinct categories of ViT PTQ baselines: (1) scaling factor optimization (PTQ4ViT [56], RepQ-ViT [28], and FIMA-Q [51]), (2) rounding function optimization (ERQ [59] and FIMA-Q [51]), (3) weight

correction (ERQ [59]), and (4) activation distribution shaping (NoisyQuant [34]) to reduce quantization error. Additionally, for CLIP and SigLIP models, prefixes are inserted from the searched layer to the final layer. DINOv2, trained in a self-supervised manner, exhibits different behavior compared to CLIP and SigLIP models; consequently,

Table 4. **VLM performance.** We evaluate our method on image and video benchmarks using Qwen3-VL- $\{2B,8B\}$ models under 4-bit quantization.

Method	Qwen3-VL-2B				Qwen3-VL-8B			
	Image		Video		Image		Video	
	GQA	VQAv2	Video-MME	MLVU	GQA	VQAv2	Video-MME	MLVU
Full-precision	58.59	77.05	73.44	68.34	59.04	77.86	78.78	78.19
Naïve	27.12	10.86	32.11	37.40	22.32	26.14	35.33	39.33
RepQ-ViT	38.77	32.03	44.56	41.17	37.84	46.29	50.44	44.89
w/ RegCache	42.11 (+3.34)	42.72 (+10.69)	49.22 (+4.66)	43.47 (+2.30)	44.00 (+6.16)	50.44 (+4.15)	52.89 (+2.45)	45.40 (+0.51)

Table 5. Zero-shot classification accuracy (%) on various datasets.

Model	Method	StanfordCars	Flowers-102	Food-101	CIFAR-100	Caltech101	OxfordIIIPet	DTD
CLIP-B/16	FP32	64.41	65.88	85.22	68.44	85.82	88.03	44.31
	Naïve	29.76	26.20	33.30	35.96	70.59	74.19	30.05
	w/ RegCache	49.96 (+20.20)	55.39 (+29.19)	74.68 (+41.38)	51.87 (+15.91)	83.22 (+12.63)	86.21 (+12.02)	42.82 (+12.77)
OpenCLIP-B/16	FP32	88.07	69.88	83.77	76.82	88.37	88.74	54.89
	Naïve	74.85	42.97	36.44	40.61	75.44	78.09	36.28
	w/ RegCache	85.85 (+11.00)	68.06 (+25.09)	80.80 (+44.36)	71.73 (+31.12)	86.88 (+11.44)	87.00 (+8.91)	51.70 (+15.42)
SigLIP-B/16	FP32	90.81	82.63	89.34	72.33	93.10	92.15	63.51
	Naïve	87.97	75.26	78.31	54.79	92.65	90.24	62.82
	w/ RegCache	89.73 (+1.76)	80.32 (+5.06)	88.17 (+9.86)	66.87 (+12.08)	92.65 (+0.00)	91.33 (+1.09)	63.62 (+0.80)
SigLIP2-B/16	FP32	92.74	83.38	90.65	77.10	93.19	92.31	61.33
	Naïve	35.12	26.38	30.55	20.92	67.48	58.22	37.23
	w/ RegCache	88.20 (+53.08)	76.50 (+50.12)	86.47 (+55.92)	59.78 (+38.86)	92.26 (+24.78)	89.70 (+31.48)	57.77 (+20.54)

we find that inserting the prefix only at the searched layer yields better results.

Further details on the setup can be found in Sec. E.

5.2. Main results

Standalone vision encoders. In Tab. 2, we report the zero-shot image classification accuracy on ImageNet-1k dataset. We observe that the baselines combined with the RegCache consistently achieve better accuracy in most settings. Specifically, baselines with RegCache outperform the base quantization methods in terms of both best accuracy gap (Best Δ) and average accuracy gap (Average Δ). Only one setup—DINOv2—exhibits a negligible accuracy drop.

For zero-shot image–text retrieval (Tab. 3), we observe that RegCache consistently improves performance across all setups. These results indicate RegCache can integrate well with other quantization methods across diverse tasks.

In particular, RegCache provides greater benefits when applied to low precision quantization settings (i.e., 4-bit and 6-bit), because the impact of activation outliers on quantization becomes correspondingly more severe.

Vision-language models. We further evaluate our quantized vision encoders within VLMs on image and video

benchmarks (Tab. 4). All results are reported in the 4-bit setting on top of the PTQ baseline (RepQ-ViT), reflecting highly constrained deployment setting. As shown in Tab. 4, RegCache consistently improves accuracy in VLMs, demonstrating robust gains across benchmarks.

Universality of prefixes. Since the prefix search procedure in RegCache involves validation on the training split of the ImageNet-1k dataset, we additionally assess whether the learned prefixes generalize to other datasets, as the register token might have overfit to ImageNet-1k. In this spirit, we perform zero-shot classification on other datasets, with the results reported in Tab. 5. These results indicate that the prefix learned on ImageNet-1k remains effective on other datasets, suggesting that it acts as a universal register token.

5.3. Analyses

Outlier reduction. Tab. 7 illustrates the change in the maximum token norm of the quantization-sensitive layer input when RegCache is applied. As expected, the maximum token norm decreases: This reduction effectively narrows the dynamic range of quantization, thereby improving quantization performance.

Table 6. **Latency results.** We measure the latency (ms) of each model on a single NVIDIA A6000 GPU using TensorRT [39, 40]. (a) Standalone vision encoder latency for CLIP-B/16 and SigLIP-B/16. (b) Vision encoder (VE) and language model (LM) prefill latency on Qwen3-VL-2B. We also report the end-to-end speedup (Accel.) achieved by quantizing only the vision encoder, while the LM quantized to INT8.

(a) Standalone VE. Batch size: 64.				(b) Qwen3-VL-2B				
Model	Method	Latency (ms)	Accel.	Data	Method	VE (ms)	LM Prefill (ms)	Accel.
CLIP-B/16	Full-precision	132.13	–	Image	Full-precision	30.21	51.76	–
	INT8	60.64	2.18×		INT8	8.33	11.63	2.10×
	INT8 + RegCache	61.27 (+1.04%)	2.16×		INT8 + RegCache	8.40 (+0.80%)	11.81	2.08×
SigLIP-B/16	Full-precision	128.49	–	Video	Full-precision	79.18	124.00	–
	INT8	62.29	2.06×		INT8	10.43	27.91	2.79×
	INT8 + RegCache	63.25 (+1.54%)	2.03×		INT8 + RegCache	10.44 (+0.01%)	27.98	2.79×

Table 7. **Reduction in maximum token norm within the input of quantization-sensitive layers in W8A8.** We report the mean across 500 image samples.

Model	Max token	
	Vanilla	w/ RegCache
CLIP	41.38	11.45
OpenCLIP	92.78	9.64
SigLIP	35.82	3.64
SigLIP2	148.20	15.16

Table 8. **Ablation studies.** We compare the contribution of each component of RegCache on SigLIP-B/16 and SigLIP2-B/16. Caching and deleting plays a complementary role, enabling a wide coverage over a wide range of vision encoders.

Method	SigLIP-B/16	SigLIP2-B/16
Baseline	69.71	26.04
Prefix Caching	74.37	23.82
Token Deleting	42.41	69.06
Prefix Caching + Token Deleting	74.38	72.35

Ablation. To support our design choices, we ablate two components of RegCache: (1) prefix caching and (2) token deleting. In Tab. 8, we present the ablation study results for SigLIP and SigLIP2. The results show that the two stages, prefix caching and token deleting, act synergistically, yielding the best performance when both components are used together for both vision encoders. Surprisingly, when only one of the two steps is applied, we obtain even worse results than in the naïve case, further supporting the validity of our design choice.

5.4. Latency

We measure latency for both standalone vision encoders (Tab. 6a) and VLMs (Tab. 6b), and find that RegCache adds only marginal overhead (up to 1.54%). For VLMs, we profile time-to-first-token (TTFT): quantizing the vision en-

coder yields over a 2× TTFT reduction with the LLM quantized to INT8, indicating that the vision encoder becomes the primary bottleneck once the LLM is accelerated. We further observe that this acceleration is even more pronounced for video inputs, where processing multiple frames incurs substantial compute.

5.5. Other experiments

Beyond the main experiments, we conduct additional experiments as follows, which will be presented in the supplementary materials:

- Retrieval results with other vision encoders ▷ Sec. C
- Visualization of searched register tokens ▷ Sec. G
- Token deletion effect analysis with segmentation task ▷ Sec. H
- Layerwise sensitivity to the prefix-insertion layer ▷ Sec. J
- RegCache using reconstruction loss ▷ Sec. K
- Using FP16 instead of token deleting ▷ Sec. L
- Combining with weight-only quantization ▷ Sec. N
- Combining with Hadamard rotation algorithms ▷ Sec. O
- Combining with LLM outlier-mitigation methods ▷ Sec. P

6. Conclusion

In this paper, we introduce a training-free outlier mitigation algorithm, *RegCache*. RegCache can serve as an on-top method, and it can be combined with existing PTQ algorithms for large-scale transformer-based vision encoders. Through extensive experiments, we demonstrate that RegCache consistently improves quantization performance across various tasks, indicating that it is indeed synergistic with other quantization methods. Our analyses reveal that RegCache effectively suppresses activation outliers in quantization-sensitive layers, thereby narrowing the dynamic range of the input and improving quantization performance. Furthermore, we take a step toward identifying

register tokens that are optimal for the quantization of vision encoders—a task that is inherently more elusive than for language models.

Limitations. A major limitation of our method is the need to tune several additional hyperparameters, such as the maximum number of tokens to delete and the number of prefix tokens. Another limitation is that the number of prefix and deleted tokens must be selected heuristically for each vision encoder and base quantization algorithm.

Discussions and future directions. Our work covers a variety of vision encoders, including those trained on multimodal data (e.g., CLIP) and those trained on vision-only data (e.g., DINOv2). In our experiments, we observe that quantization-related measures (e.g., quantization sensitivity) behave somewhat differently across these cases, warranting further study. Another research direction arises from the differences between LLMs and ViT-based vision encoders: their outlier behavior differs significantly (see Sec. M for an extended discussion). Understanding this phenomenon would benefit a wide range of domains, including quantization and representation learning.

Acknowledgment

This work was supported in part by AI Research Hub Project (No.RS-2024-00457882) and in part by Institute of Information & communications Technology Planning & Evaluation (IITP) grant funded by the Korea government (MSIT) (No.RS-2019-II191906, Artificial Intelligence Graduate School Program (POSTECH)).

References

- [1] Saleh Ashkboos, Amirkeivan Mohtashami, Maximilian L Croci, Bo Li, Pashmina Cameron, Martin Jaggi, Dan Alishtarh, Torsten Hoefler, and James Hensman. QuaRot: Outlier-free 4-bit inference in rotated llms. *Advances in Neural Information Processing Systems*, 2024. 27
- [2] Shuai Bai, Yuxuan Cai, Ruizhe Chen, Keqin Chen, Xionghui Chen, Zesen Cheng, Lianghao Deng, Wei Ding, Chang Gao, Chunjiang Ge, et al. Qwen3-vl technical report. *arXiv preprint arXiv:2511.21631*, 2025. 6, 16
- [3] Lucas Beyer, Andreas Steiner, André Susano Pinto, Alexander Kolesnikov, Xiao Wang, Daniel Salz, Maxim Neumann, Ibrahim Alabdulmohsin, Michael Tschannen, Emanuele Bugliarello, et al. Paligemma: A versatile 3b vlm for transfer. *arXiv preprint arXiv:2407.07726*, 2024. 1
- [4] Daniel Bolya, Po-Yao Huang, Peize Sun, Jang Hyun Cho, Andrea Madotto, Chen Wei, Tengyu Ma, Jiale Zhi, Jathushan Rajasegaran, Hanoona Abdul Rasheed, Junke Wang, Marco Monteiro, Hu Xu, Shiyu Dong, Nikhila Ravi, Shang-Wen Li, Piotr Dollar, and Christoph Feichtenhofer. Perception encoder: The best visual embeddings are not at the output of the network. In *The Thirty-ninth Annual Conference on Neural Information Processing Systems*, 2025. 20
- [5] Yelysei Bondarenko, Markus Nagel, and Tijmen Blankevoort. Understanding and overcoming the challenges of efficient transformer quantization. In *Empirical Methods in Natural Language Processing*, 2021. 2
- [6] Lukas Bossard, Matthieu Guillaumin, and Luc Van Gool. Food-101—mining discriminative components with random forests. In *European conference on computer vision*, 2014. 6
- [7] Mengzhao Chen, Yi Liu, Jiahao Wang, Yi Bin, Wenqi Shao, and Ping Luo. PrefixQuant: Eliminating outliers by prefixed tokens for large language models quantization. *arXiv preprint arXiv:2410.05265*, 2024. 2
- [8] Mehdi Cherti, Romain Beaumont, Ross Wightman, Mitchell Wortsman, Gabriel Ilharco, Cade Gordon, Christoph Schuhmann, Ludwig Schmidt, and Jenia Jitsev. Reproducible scaling laws for contrastive language-image learning. In *Proceedings of the IEEE/CVF conference on computer vision and pattern recognition*, 2023. 6
- [9] Yoni Choukroun, Eli Kravchik, Fan Yang, and Pavel Kisilev. Low-bit quantization of neural networks for efficient inference. In *IEEE/CVF International Conference on Computer Vision Workshop*, 2019. 1
- [10] M. Cimpoi, S. Maji, I. Kokkinos, S. Mohamed, , and A. Vedaldi. Describing textures in the wild. In *Proceedings of the IEEE Conf. on Computer Vision and Pattern Recognition (CVPR)*, 2014. 6
- [11] Timothée Darcet, Maxime Oquab, Julien Mairal, and Piotr Bojanowski. Vision transformers need registers. In *International Conference on Learning Representations*, 2024. 2, 3, 19, 25
- [12] Jia Deng, Wei Dong, Richard Socher, Li-Jia Li, Kai Li, and Li Fei-Fei. ImageNet: A large-scale hierarchical image database. In *IEEE conference on computer vision and pattern recognition*, 2009. 6

- [13] Tim Dettmers, Mike Lewis, Younes Belkada, and Luke Zettlemoyer. GPT3.int8(): 8-bit matrix multiplication for transformers at scale. In *Advances in neural information processing systems*, 2022. 2
- [14] Alexey Dosovitskiy, Lucas Beyer, Alexander Kolesnikov, Dirk Weissenborn, Xiaohua Zhai, Thomas Unterthiner, Mostafa Dehghani, Matthias Minderer, Georg Heigold, Sylvain Gelly, Jakob Uszkoreit, and Neil Houlsby. An image is worth 16x16 words: Transformers for image recognition at scale. In *International Conference on Learning Representations*, 2021. 1
- [15] Abhimanyu Dubey, Abhinav Jauhri, Abhishek Pandey, Abhishek Kadian, Ahmad Al-Dahle, Aiesha Letman, Akhil Mathur, Alan Schelten, Aobo Yang, Angela Fan, et al. The llama 3 herd of models. *arXiv preprint arXiv:2407.21783*, 2024. 25
- [16] Fartash Faghri, Pavan Kumar Anasosalu Vasu, Cem Koc, Vaishaal Shankar, Alexander T Toshev, Oncel Tuzel, and Hadi Pouransari. MobileCLIP2: Improving multi-modal reinforced training. *Transactions on Machine Learning Research*, 2025. 1
- [17] Li Fei-Fei, Rob Fergus, and Pietro Perona. Learning generative visual models from few training examples: An incremental bayesian approach tested on 101 object categories. In *conference on computer vision and pattern recognition workshop*, 2004. 6
- [18] Chaoyou Fu, Yuhan Dai, Yongdong Luo, Lei Li, Shuhuai Ren, Renrui Zhang, Zihan Wang, Chenyu Zhou, Yunhang Shen, Mengdan Zhang, et al. Video-MME: The first-ever comprehensive evaluation benchmark of multi-modal llms in video analysis. In *CVPR*, 2025. 6
- [19] Yash Goyal, Tejas Khot, Douglas Summers-Stay, Dhruv Batra, and Devi Parikh. Making the V in VQA matter: Elevating the role of image understanding in Visual Question Answering. In *Conference on Computer Vision and Pattern Recognition (CVPR)*, 2017. 6
- [20] Xiangming Gu, Tianyu Pang, Chao Du, Qian Liu, Fengzhuo Zhang, Cunxiao Du, Ye Wang, and Min Lin. When attention sink emerges in language models: An empirical view. In *International Conference on Learning Representations*, 2025. 25
- [21] Zhiyu Guo, Hidetaka Kamigaito, and Taro Watanabe. Attention score is not all you need for token importance indicator in kv cache reduction: Value also matters. In *Empirical Methods in Natural Language Processing*, 2024. 2
- [22] Drew A Hudson and Christopher D Manning. GQA: A new dataset for real-world visual reasoning and compositional question answering. *Conference on Computer Vision and Pattern Recognition (CVPR)*, 2019. 6
- [23] Nicholas Jiang, Amil Dravid, Alexei A Efros, and Yossi Gandelsman. Vision transformers don't need trained registers. In *Advances in neural information processing systems*, 2025. 2, 14, 19, 20
- [24] Seil Kang, Jinyeong Kim, Junhyeok Kim, and Seong Jae Hwang. See what you are told: Visual attention sink in large multimodal models. In *International Conference on Learning Representations*, 2025. 2
- [25] Olga Kovaleva, Saurabh Kulshreshtha, Anna Rogers, and Anna Rumshisky. BERT busters: Outlier dimensions that disrupt transformers. In *Findings of the ACL*, 2021. 2
- [26] Jonathan Krause, Michael Stark, Jia Deng, and Li Fei-Fei. 3d object representations for fine-grained categorization. In *Proceedings of the IEEE international conference on computer vision workshops*, 2013. 6
- [27] Yanwei Li, Chengyao Wang, and Jiaya Jia. Llama-vid: An image is worth 2 tokens in large language models. In *European Conference on Computer Vision*, 2024. 1
- [28] Zhikai Li, Junrui Xiao, Lianwei Yang, and Qingyi Gu. RepQ-ViT: Scale reparameterization for post-training quantization of vision transformers. In *Proceedings of the IEEE/CVF International Conference on Computer Vision*, 2023. 1, 3, 7, 17
- [29] Ji Lin, Jiaming Tang, Haotian Tang, Shang Yang, Wei-Ming Chen, Wei-Chen Wang, Guangxuan Xiao, Xingyu Dang, Chuang Gan, and Song Han. AWQ: Activation-aware weight quantization for on-device LLM compression and acceleration. In *Proceedings of Machine Learning and Systems*, 2024. 2, 26
- [30] Tsung-Yi Lin, Michael Maire, Serge Belongie, James Hays, Pietro Perona, Deva Ramanan, Piotr Dollár, and C Lawrence Zitnick. Microsoft coco: Common objects in context. In *European conference on computer vision*, 2014. 6
- [31] Haotian Liu, Chunyuan Li, Qingyang Wu, and Yong Jae Lee. Visual instruction tuning. *Advances in neural information processing systems*, 2023. 1, 6
- [32] Haotian Liu, Chunyuan Li, Yuheng Li, and Yong Jae Lee. Improved baselines with visual instruction tuning. In *Proceedings of the IEEE/CVF conference on computer vision and pattern recognition*, pages 26296–26306, 2024. 16
- [33] Haotian Liu, Chunyuan Li, Yuheng Li, Bo Li, Yuanhan Zhang, Sheng Shen, and Yong Jae Lee. Llava-next: Improved reasoning, ocr, and world knowledge, 2024. 16
- [34] Yijiang Liu, Huanrui Yang, Zhen Dong, Kurt Keutzer, Li Du, and Shanghang Zhang. NoisyQuant: Noisy bias-enhanced post-training activation quantization for vision transformers. In *Proceedings of the IEEE/CVF Conference on Computer Vision and Pattern Recognition*, 2023. 3, 7, 17
- [35] Zhenhua Liu, Yunhe Wang, Kai Han, Wei Zhang, Siwei Ma, and Wen Gao. Post-training quantization for vision transformer. *Advances in Neural Information Processing Systems*, 2021. 3
- [36] Zechun Liu, Changsheng Zhao, Igor Fedorov, Bilge Soran, Dhruv Choudhary, Raghuraman Krishnamoorthi, Vikas Chandra, Yuandong Tian, and Tijmen Blankevoort. SpinQuant: LLM quantization with learned rotations. In *International Conference on Learning Representations*, 2025. 27
- [37] Andrew Lu, Wentinn Liao, Liuhui Wang, Huzheng Yang, and Jianbo Shi. Artifacts and attention sinks: Structured approximations for efficient vision transformers. *arXiv preprint arXiv:2507.16018*, 2025. 2
- [38] Maria-Elena Nilsback and Andrew Zisserman. Automated flower classification over a large number of classes. In *Indian conference on computer vision, graphics & image processing*, 2008. 6

- [39] NVIDIA Corporation. Nvidia tensorrt. <https://developer.nvidia.com/tensorrt>, . 9
- [40] NVIDIA Corporation. Deploying hugging face llava1.5-7b model in triton. https://docs.nvidia.com/deeplearning/triton-inference-server/user-guide/docs/tutorials/Popular_Models_Guide/Llava1.5/llava_trtllm_guide.html, . 9
- [41] Maxime Oquab, Timothée Darcet, Théo Moutakanni, Huy V. Vo, Marc Szafraniec, Vasil Khalidov, Pierre Fernandez, Daniel HAZIZA, Francisco Massa, Alaaeldin El-Nouby, Mido Assran, Nicolas Ballas, Wojciech Galuba, Russell Howes, Po-Yao Huang, Shang-Wen Li, Ishan Misra, Michael Rabbat, Vasu Sharma, Gabriel Synnaeve, Hu Xu, Herve Jegou, Julien Mairal, Patrick Labatut, Armand Joulin, and Piotr Bojanowski. DINOv2: Learning robust visual features without supervision. *Transactions on Machine Learning Research*, 2024. 1, 6
- [42] Omkar M. Parkhi, Andrea Vedaldi, Andrew Zisserman, and C. V. Jawahar. Cats and dogs. In *IEEE Conference on Computer Vision and Pattern Recognition*, 2012. 6
- [43] Alec Radford, Jong Wook Kim, Chris Hallacy, Aditya Ramesh, Gabriel Goh, Sandhini Agarwal, Girish Sastry, Amanda Askell, Pamela Mishkin, Jack Clark, et al. Learning transferable visual models from natural language supervision. In *International conference on machine learning*, 2021. 1, 6
- [44] Oriane Siméoni, Huy V Vo, Maximilian Seitzer, Federico Baldassarre, Maxime Oquab, Cijo Jose, Vasil Khalidov, Marc Szafraniec, Seungeun Yi, Michaël Ramamonjisoa, et al. Dinov3. *arXiv preprint arXiv:2508.10104*, 2025. 2
- [45] Seungwoo Son, Wonpyo Park, Woohyun Han, Kyuyeon Kim, and Jaeho Lee. Prefixing attention sinks can mitigate activation outliers for large language model quantization. In *Empirical Methods in Natural Language Processing*, 2024. 2, 3, 5
- [46] Mingjie Sun, Xinlei Chen, J Zico Kolter, and Zhuang Liu. Massive activations in large language models. In *Conference on Language Modeling*, 2024. 2, 3, 25
- [47] Yu-Shan Tai et al. MPTQ-ViT: Mixed-precision post-training quantization for vision transformer. *arXiv preprint arXiv:2401.14895*, 2024. 28
- [48] William Timkey and Marten Van Schijndel. All bark and no bite: Rogue dimensions in transformer language models obscure representational quality. In *Empirical Methods in Natural Language Processing*, 2021. 2
- [49] Michael Tschannen, Alexey Gritsenko, Xiao Wang, Muhammad Ferjad Naeem, Ibrahim Alabdulmohsin, Nikhil Parthasarathy, Talfan Evans, Lucas Beyer, Ye Xia, Basil Mustafa, et al. SigLIP 2: Multilingual vision-language encoders with improved semantic understanding, localization, and dense features. *arXiv preprint arXiv:2502.14786*, 2025. 6
- [50] Pavan Kumar Anasosalu Vasu, Fartash Faghri, Chun-Liang Li, Cem Koc, Nate True, Albert Antony, Gokula Santhanam, James Gabriel, Peter Grasch, Oncel Tuzel, et al. Fastvlm: Efficient vision encoding for vision language models. In *Proceedings of the Computer Vision and Pattern Recognition Conference*, 2025. 1
- [51] Zhuguanyu Wu, Shihe Wang, Jiayi Zhang, Jiaxin Chen, and Yunhong Wang. FIMA-Q: Post-training quantization for vision transformers by fisher information matrix approximation. In *Proceedings of the Computer Vision and Pattern Recognition Conference*, 2025. 1, 3, 7, 17
- [52] Guangxuan Xiao, Ji Lin, Mickael Seznec, Hao Wu, Julien Demouth, and Song Han. SmoothQuant: Accurate and efficient post-training quantization for large language models. In *International conference on Machine Learning*, 2023. 2
- [53] Guangxuan Xiao, Yuandong Tian, Beidi Chen, Song Han, and Mike Lewis. Efficient streaming language models with attention sinks. In *International Conference on Learning Representations*, 2024. 2
- [54] Kai Yuanqing Xiao, Logan Engstrom, Andrew Ilyas, and Aleksander Madry. Noise or signal: The role of image backgrounds in object recognition. In *International Conference on Learning Representations*, 2021. 4
- [55] Jaewoo Yang, Hayun Kim, and Younghoon Kim. Mitigating quantization errors due to activation spikes in GLU-based LLMs. *arXiv preprint 2405.14428*, 2024. 2
- [56] Zhihang Yuan, Chenhao Xue, Yiqi Chen, Qiang Wu, and Guangyu Sun. PTQ4ViT: Post-training quantization for vision transformers with twin uniform quantization. In *European conference on computer vision*, 2022. 3, 7, 17
- [57] Xiaohua Zhai, Basil Mustafa, Alexander Kolesnikov, and Lucas Beyer. Sigmoid loss for language image pre-training. In *Proceedings of the IEEE/CVF international conference on computer vision*, 2023. 6
- [58] Tianchen Zhao, Tongcheng Fang, Haofeng Huang, Rui Wan, Widyadewi Soedarmadji, Enshu Liu, Shiyao Li, Zinan Lin, Guohao Dai, Shengen Yan, Huazhong Yang, Xuefei Ning, and Yu Wang. ViDiT-Q: Efficient and accurate quantization of diffusion transformers for image and video generation. In *International Conference on Learning Representations*, 2025. 27
- [59] Yunshan Zhong, You Huang, Jiawei Hu, Yuxin Zhang, and Rongrong Ji. Towards accurate post-training quantization of vision transformers via error reduction. *IEEE Trans. Pattern Anal. Mach. Intell.*, 2025. 1, 3, 7, 17
- [60] Bolei Zhou, Hang Zhao, Xavier Puig, Sanja Fidler, Adela Barriuso, and Antonio Torralba. Scene parsing through ade20k dataset. In *Proceedings of the IEEE Conference on Computer Vision and Pattern Recognition*, 2017. 20
- [61] Junjie Zhou, Yan Shu, Bo Zhao, Boya Wu, Zhengyang Liang, Shitao Xiao, Minghao Qin, Xi Yang, Yongping Xiong, Bo Zhang, et al. MLVU: Benchmarking multi-task long video understanding. In *Proceedings of the IEEE/CVF Conference on Computer Vision and Pattern Recognition*, 2025. 6

Appendix

A. Additional Results on Quantization Sensitivity

In this section, we provide additional plots for other vision encoders, analogous to those in Figure 3. In Fig. 6, we plot layerwise quantization sensitivity (top row) and maximum token norm (bottom row) for OpenCLIP and SigLIP2. The trends are consistent with our analysis in Sec. 3.1: increases in maximum token norm coincide with decreases in quantization sensitivity. However, in the case of SigLIP2, the absolute scale of the maximum norm is significantly larger than in the other architectures we considered. Consequently, applying RegCache yields a clearer benefit, as shown in Tab. 2. Given SigLIP2’s distinct behavior compared to other vision encoders, it would be intriguing to investigate further; we leave this for future work.

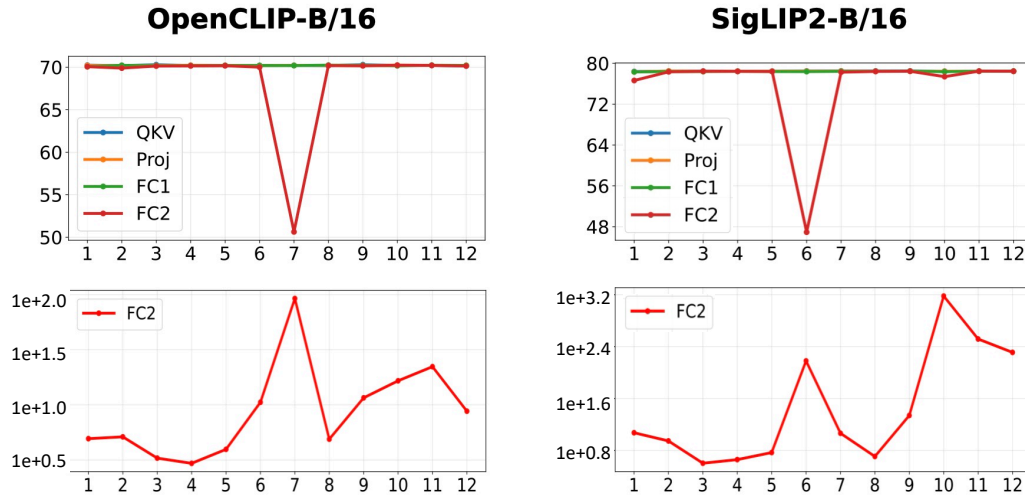


Figure 6. **(Top) Layerwise quantization sensitivity (%)**. Zero-shot ImageNet-1k accuracy when we quantize only one layer to W8A8. **(Bottom) Layerwise max token norms**. The largest ℓ_∞ -norm of all tokens in an image on a logarithmic scale, averaged over the ImageNet-1k validation set.

B. Comparison with Test-Time Registers

Our experimental results demonstrate that RegCache consistently outperforms the test-time register [23] variant in quantization settings. As discussed in Sec. 2, Jiang et al. [23] propose register tokens as a concurrent approach to mitigating activation outliers. In an extended experiment reported in Appendix 2 (Ver. 5 [23]), they further inject test-time registers as a form of KV cache while zeroing out outlier neurons, showing that high-norm residual-stream outliers can be suppressed. To assess the practical utility of this mechanism in quantized models, we evaluate it under identical conditions and compare it directly with RegCache.

The results show that RegCache remains consistently superior, suggesting that identifying the optimal curation tailored to a quantization-based setup is more effective than relying on test-time register based outlier suppression mechanism.

Table 9. **Comparison with test-time register.** Accuracy of zero-shot image classification on ImageNet-1k under W8A8 quantization.

Method	CLIP-B/16	SigLIP-B/16
FP32	68.32	76.05
Naïve	34.01	69.71
Test-time register	44.30	73.81
RegCache	59.71	74.38

C. Additional Results on Image Retrieval

We present supplementary tables for additional vision encoders, in a format consistent with Tab. 3. For other models, Tab. 10 presents zero-shot image–text retrieval results on the MS-COCO dataset for OpenCLIP and SigLIP2. In both models, RegCache consistently achieves the highest retrieval accuracy as well.

Table 10. **Zero-shot image–text retrieval performance of OpenCLIP and SigLIP2 on MS-COCO (R@1)**. The best results are marked in **bold**. Best/Average Δ denote the maximum/average accuracy gaps between each baseline and its RegCache counterpart, excluding the Naïve cases.

	OpenCLIP-B/16						SigLIP2-B/16					
	Image \rightarrow Text			Text \rightarrow Image			Image \rightarrow Text			Text \rightarrow Image		
	W4A4	W6A6	W8A8									
FP32	61.02	61.02	61.02	41.38	41.38	41.38	71.60	71.60	71.60	52.33	52.33	52.33
Naïve	0.02	0.16	37.32	0.03	0.24	26.30	0.02	0.02	14.26	0.02	0.16	13.86
w/ RegCache	0.00	0.32	57.60	0.04	0.77	38.45	0.02	0.08	64.02	0.03	0.22	46.80
PTQ4ViT	0.04	50.60	59.60	0.06	34.56	40.66	0.04	29.88	69.74	0.19	27.33	51.62
w/ RegCache	1.00	60.00	60.00	3.00	40.96	40.96	0.70	53.90	70.12	2.64	39.96	51.68
RepQ-ViT	0.12	17.60	57.62	0.21	8.90	38.88	0.16	57.00	69.20	0.28	39.20	50.15
w/ RegCache	1.56	32.96	59.44	1.38	14.90	39.82	3.20	58.78	69.76	3.49	41.26	50.15
NoisyQuant	0.46	43.86	53.84	1.20	27.05	34.50	0.07	28.74	62.04	0.65	25.28	46.32
w/ RegCache	2.18	51.58	56.06	2.81	31.73	35.53	0.32	50.66	70.24	1.79	39.25	51.41
FIMA-Q	55.82	58.84	59.26	38.02	40.39	40.21	67.70	67.68	67.70	47.22	47.21	47.22
w/ RegCache	57.34	59.88	59.86	40.02	40.30	40.58	71.54	71.54	71.52	52.49	52.49	52.50
ERQ	9.70	32.56	58.74	4.28	14.74	39.83	8.28	64.80	69.76	5.78	45.44	49.97
w/ RegCache	13.02	33.64	59.56	5.19	15.38	40.04	12.30	65.56	70.00	9.18	46.28	50.20
Best Δ	+3.32	+15.36	+2.22	+2.94	+6.40	+1.03	+4.02	+24.02	+8.20	+5.27	+13.97	+5.28
Average Δ	+1.79	+6.92	+1.17	+1.73	+3.53	+0.57	+2.36	+10.47	+2.64	+3.09	+6.96	+2.13

D. Additional Results on VLMs

We further evaluate RegCache on the widely adopted LLaVA family [32, 33] on the GQA and VQAv2 benchmarks, as summarized in Tab. 11. In Tab. 4, we consider a practical deployment setting with 4-bit quantization and RepQ-ViT as the PTQ baseline. We note that RepQ-ViT is particularly effective in practice, offering both favorable accuracy gains and low calibration overhead, especially for larger vision encoders in VLMs. Consistent with our observations on Qwen3 [2], RegCache delivers stable gains in this setting, confirming that its efficacy extends beyond a specific architecture.

Table 11. VLM performance on LLaVA architecture-based models under 4-bit quantization.

(a) LLaVA-1.5 models.				
Method	LLaVA-1.5-7B		LLaVA-1.5-13B	
	GQA	VQAv2	GQA	VQAv2
FP32	60.78	76.64	62.57	78.29
Naïve	33.84	35.62	34.70	35.89
RepQ-ViT	41.40	45.87	43.27	47.85
w/ RegCache	45.10 (+3.70)	50.11 (+4.24)	46.21 (+2.94)	52.15 (+4.30)

(b) LLaVA-NeXT models.				
Method	LLaVA-1.6-vicuna-13B		LLaVA-1.6-mistral-7B	
	GQA	VQAv2	GQA	VQAv2
FP32	63.08	79.33	56.59	76.15
Naïve	35.72	36.70	31.87	35.21
RepQ-ViT	48.93	56.70	44.63	53.45
w/ RegCache	51.40 (+2.47)	58.83 (+2.13)	46.21 (+1.58)	55.64 (+2.19)

E. Experimental Settings and Baselines

In this section, we provide additional details on the vision encoder models, quantization baselines, and the hardware setup used in our experiments.

Models. The vision encoders we choose cover a broad range of training objectives (image–text contrastive learning vs. self-supervised learning) and architectural choices for global feature aggregation, providing a diverse testbed for evaluating RegCache. CLIP and SigLIP are trained on image–text pairs with contrastive objectives, whereas DINOv2 is trained on image-only datasets. Regarding input tokens, CLIP and DINOv2 utilize a class token to extract global features, while SigLIP and SigLIP2 use patch-wise pooling to generate a token that captures global information.

Baselines. We consider the following baselines ranging from widely used to recent:

- **PTQ4ViT** [56] proposes a twin uniform quantizer to handle the unbalanced activation distributions found in ViTs, particularly after non-linearities such as Softmax and GELU.
- **RepQ-ViT** [28] addresses quantization bottlenecks by applying specialized preprocessing to sensitive layers, such as channel-wise quantization after LayerNorm and log2 quantization after Softmax.
- **NoisyQuant** [34] introduces a quantizer-agnostic strategy that adds fixed uniform bias to activations, thereby reducing the quantization error of heavy-tailed distributions.
- **FIMA-Q** [51] suggests optimizing the rounding function and scaling factor using effective Hessian-guided quantization loss.
- **ERQ** [59] decouples activation and weight error reduction via Ridge-regression-based weight correction. It also integrates several effective PTQ techniques, including incorporating channel-wise scaling factors into the LayerNorm parameters to handle activation outliers, and applying group-wise uniform quantization with separate quantizers for weight outliers, along with rounding function optimization.

All baselines use per-tensor dynamic quantization with 8-/6-/4-bit integer precision. Following the original papers, we use 1,024 calibration samples for NoisyQuant and 32 calibration samples for RepQ-ViT, PTQ4ViT, and ERQ. For FIMA-Q, we use 1,024 samples for optimization and 128 samples for calibration.

Hardware. Most standalone vision encoder experiments are conducted on NVIDIA RTX 4090 GPUs, whereas VLM evaluations are performed on NVIDIA RTX A6000 GPUs. Due to its large memory requirements, the FIMA-Q baseline is evaluated on both NVIDIA RTX A6000 and NVIDIA A100 80GB GPUs.

F. High Cosine Similarity of Outlier Tokens

In this section, we provide a simple explanation for why outlier tokens maintain high cosine similarity across images, as shown in Tab. 1.

As a stylized example, consider two distinct outlier tokens, each modeled as a “spiked” vector in which a single element has high magnitude (i.e., C in Lemma 1). Lemma 1 says that the high cosine similarity over the outlier tokens can largely be attributed to two factors⁵: **(i) the presence of large-magnitude entries** and **(ii) the alignment of the corresponding entry indices (i.e., same or at least similar channels)**.

Lemma 1. *Let $\mathbf{x}, \mathbf{y} \in \mathbb{R}^d$ and fix an index $i \in \{1, \dots, d\}$. Moreover, let $\mathbf{1}_i \in \mathbb{R}^d$ denote the one-hot vector whose i th entry is 1 and all other entries are 0. For $C \in \mathbb{R}^+$, define $\mathbf{x}' = \mathbf{x} + C\mathbf{1}_i$, $\mathbf{y}' = \mathbf{y} + C\mathbf{1}_i$. Then the vectors asymptotically converge to each other, i.e.,*

$$\lim_{C \rightarrow \infty} \frac{\langle \mathbf{x}', \mathbf{y}' \rangle}{\|\mathbf{x}'\|_2 \|\mathbf{y}'\|_2} = 1. \quad (3)$$

Moreover, for $\mathbf{y}'' = \mathbf{y} + C\mathbf{1}_j$, where $j \neq i$, then the vectors become asymptotically orthogonal to each other, i.e.,

$$\lim_{C \rightarrow \infty} \frac{\langle \mathbf{x}', \mathbf{y}'' \rangle}{\|\mathbf{x}'\|_2 \|\mathbf{y}''\|_2} = 0. \quad (4)$$

Proof. For the same-index case (Eq. (3)), we can write this explicitly as

$$\frac{\langle \mathbf{x}', \mathbf{y}' \rangle}{\|\mathbf{x}'\|_2 \|\mathbf{y}'\|_2} = \frac{\langle \mathbf{x}, \mathbf{y} \rangle + C(x_i + y_i) + C^2}{\sqrt{\|\mathbf{x}\|_2^2 + 2Cx_i + C^2} \sqrt{\|\mathbf{y}\|_2^2 + 2Cy_i + C^2}}, \quad (5)$$

where x_i (resp. y_i) denotes the i th entry of \mathbf{x} (resp. \mathbf{y}). Dividing numerator and denominator by C^2 , we get

$$\frac{1 + \frac{x_i + y_i}{C} + \frac{\langle \mathbf{x}, \mathbf{y} \rangle}{C^2}}{\sqrt{1 + \frac{2x_i}{C} + \frac{\|\mathbf{x}\|_2^2}{C^2}} \sqrt{1 + \frac{2y_i}{C} + \frac{\|\mathbf{y}\|_2^2}{C^2}}}. \quad (6)$$

As $C \rightarrow \infty$, all terms of order $1/C$ and $1/C^2$ vanish, and we get what we want. The case of the different-index (Eq. (4)) can be handled similarly. \square

Indeed, as shown in Fig. 2 (right), we find that across different images, outlier tokens tend to have similar magnitudes in certain coordinates (i.e., along specific channels shared across different tokens).

⁵There are some cases where each component has a small magnitude, yet the vectors are still similar to one another. In high dimensions, however, this rarely happens; for example, random vectors become almost orthogonal as the dimension tends to infinity. In vision encoders, the number of channels per token is typically large (e.g., 768 channels in CLIP and SigLIP families), which results in low similarity among non-outlier tokens (e.g., “Normal tokens” in Tab. 1).

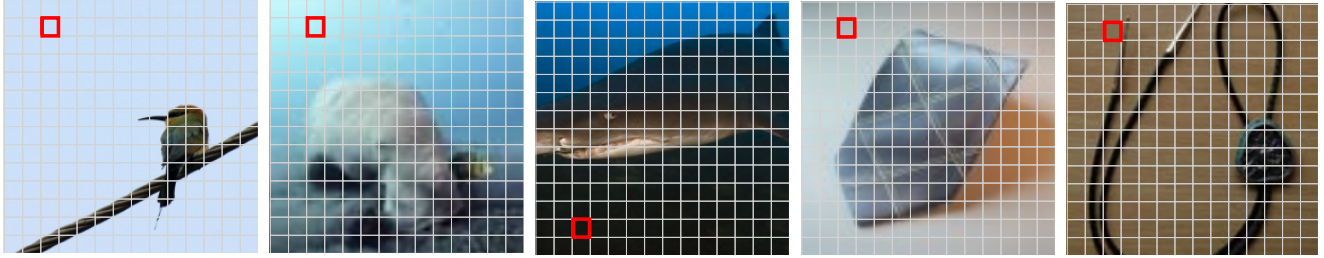


Figure 7. Visualization of curated prefix tokens from ImageNet-1k

G. Visualization of Curated Prefix Tokens

In Fig. 7, we visualize the top 5 prefix tokens selected by the method described in Sec. 4.1, ranked by their effectiveness under quantization as measured by W8A8 zero-shot classification accuracy on ImageNet-1k. The results are consistent with prior findings [11, 23], revealing that the register tokens are located in background regions. We find that the selected register tokens commonly correspond to low-frequency regions surrounded by semantically uninformative patches.

H. Segmentation Results

To analyze the impact of token deletion on dense prediction, we conduct semantic segmentation experiments on ADE20K⁶ and report the mIoU results in Tab. 12a. We find that the sink token shows a noticeably lower mIoU score, consistent with prior observations that sink tokens can degrade segmentation performance [4, 23]. To remove the sink token while maintaining spatial structure, we replace its position with an interpolated token obtained by averaging the surrounding patch embeddings, and report the resulting performance in Tab. 12b. Our method effectively suppresses the outliers induced by sink-token deletion, thereby improving post-training quantization performance on dense prediction tasks.

Table 12. **Analysis of sink tokens and RegCache for segmentation.** Results on ADE20K using W8A8 quantized SigLIP-B/16.

(a) mIoU by token		(b) Increased mIoU with RegCache	
Setting	mIoU	Method	mIoU
Sink	16.67	FP32	32.85
Random	12.02	Naïve	30.30
Non-sink	30.15	RegCache w/ interp.	32.46

⁶We use ADE20K-*MIT Scene Parsing Challenge 2016*, which is the subset of the ADE20K benchmark [60], available at <http://sceneparsing.csail.mit.edu/>.

I. Impact of Activation Outlier on Quantization

To assess the impact of outlier on quantization, we control the quantization range at the token level. In Tab. 13, “w/ outliers” applies standard per-tensor quantization. In contrast, the “w/o outliers” setting excludes outlier tokens from the per-tensor range and quantizes them separately via per-token quantization. As a result, quantizing the outlier tokens separately shows a substantial performance improvement, which demonstrates that mitigating outliers is a critical problem in quantization.

Table 13. Comparison of quantization performance w/ and w/o outlier.

Model	Full Precision	w/ outlier	w/o outlier
CLIP-B/16	68.32	34.01	55.83 (+21.82)
OpenCLIP-B/16	70.22	46.12	65.43 (+19.31)
SigLIP-B/16	76.05	69.71	74.54 (+4.83)
SigLIP2-B/16	78.47	26.04	74.54 (+48.50)
DINOv2-B/16	83.26	19.20	76.58 (+57.38)

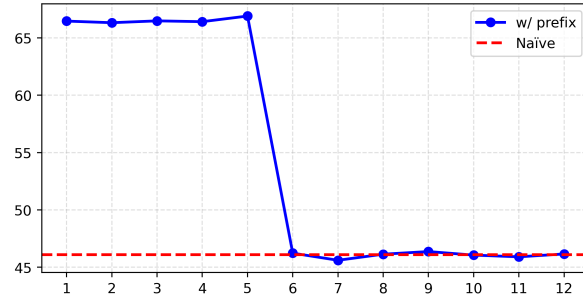


Figure 8. **Performance across prefix-insertion layers (%)**. The x-axis denotes the layer index where prefix insertion begins and the y-axis indicates zero-shot ImageNet-1k accuracy under W8A8 quantization.

J. Layerwise Sensitivity to the Prefix-insertion Layer

In Fig. 8, we visualize how accuracy changes with the layer at which prefix insertion begins. As a result, accuracy drops sharply when insertion starts at layer 6—the layer right after the quantization-sensitive layer—indicating that prefix tokens are effective only when inserted before this sensitive layer. Based on this observation, we choose the intermediate layer as an initial prefix inserting layer to minimize computational cost.

K. RegCache Selected Based on Reconstruction Loss

To further demonstrate the extensibility of our approach, we additionally evaluate a quantization reconstruction loss-based search as an alternative selection strategy. Specifically, we search for the number of prefix and deleted tokens that minimize the MSE between output features produced by FP32 processing and those produced under the quantized setting. This criterion depends only on internal activations and does not require access to target-domain labels or downstream metrics, enabling a lightweight and broadly applicable procedure.

The results in Tab. 14 show that our method remains effective under this label-free selection rule, supporting its practical deployment in scenarios where validation data is unavailable or restricted. Moreover, even without ImageNet-1k-based tuning, our method improves accuracy on average across quantization settings.

Table 14. **Results of reconstruction loss-based search.** Zero-shot classification accuracy on ImageNet-1k for various vision encoders. The best results are marked in **bold**. Best/Average Δ denote the gaps between the best/average performance of each baseline with and without RegCache, excluding the Naïve cases. Here, RegCache_{rc} denotes the results with RegCache selected based on reconstruction loss.

Method	CLIP-B/16			SigLIP-B/16		
	W4A4	W6A6	W8A8	W4A4	W6A6	W8A8
FP32		68.32			76.05	
Naïve	0.09	0.17	34.01	0.13	0.77	69.71
w/ RegCache _{rc}	0.09	0.27	59.47	0.13	23.29	74.31
PTQ4ViT	0.37	51.60	67.69	0.19	68.68	75.57
w/ RegCache _{rc}	0.32	58.33	67.77	2.19	72.27	75.93
RepQ-ViT	1.83	53.25	67.39	21.36	73.32	75.23
w/ RegCache _{rc}	15.09	66.81	68.00	30.91	74.59	75.99
NoisyQuant	0.34	46.19	63.62	1.78	71.10	75.50
w/ RegCache _{rc}	1.29	57.19	65.80	8.61	72.18	75.69
FIMA-Q	50.41	66.51	67.63	76.05	76.06	76.06
w/ RegCache _{rc}	62.27	66.90	67.78	76.12	76.12	76.12
ERQ	1.56	39.64	67.99	57.76	74.44	75.95
w/ RegCache _{rc}	47.11	65.90	68.03	60.06	75.24	76.04
Best Δ	+45.55	+26.26	+2.18	+9.55	+3.59	+0.76
Average Δ	+14.32	+11.59	+0.61	+4.15	+1.36	+0.29

L. Using FP16 Instead of Token Deletion

As a flexible variant of our method, we replace token deletion with FP16 token computation and report the results in Tab. 15. This option yields a modest accuracy improvement, but introduces a bottleneck in computing the FP16 tokens to propagate, thereby slowing down the overall process.

Table 15. **Performance of FP16 mixed precision instead of token deleting.** Accuracy of zero-shot image classification on ImageNet-1k under W8A8 quantization.

Method	SigLIP	SigLIP2
FP32	76.05	78.47
Naïve	69.71	26.04
w/ RegCache	74.38	72.35
w/ RegCache (FP16 MP)	74.51	72.82

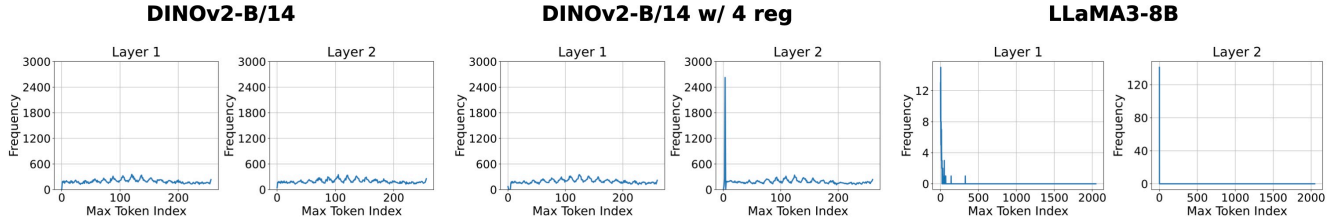


Figure 9. **The frequency of top-1 max tokens in the input tensor of FC2 layers in different models.** We evaluated DINOv2 on ImageNet-1k and LLaMA3-8B on WikiText-2 dataset.

M. Outliers in Vision Encoders vs. LLMs: A Tokenization Perspective

As shown in Fig. 3, various vision encoders exhibit outliers in the intermediate layers. Rewinding recent studies about outlier tendency in LLMs [20, 46], it is natural to ask: why do outliers consistently emerge in the intermediate layers of vision encoders, rather than in the early layers as in LLMs? In this section, we investigate this phenomenon by reconsidering the difference of *tokenization strategies* between vision encoders and LLMs.

Roughly speaking, LLMs map input sequences to tokens drawn from a discrete, fixed vocabulary. In contrast, vision encoders and other ViT-based models process inputs by mapping them to continuous token embeddings using a (convolutional) neural network. We hypothesize that differences in the emergence of sink tokens can be attributed to their fundamentally distinct tokenization process.

To test this hypothesis, we compare the outlier behavior of DINOv2, pretrained both with and without learned register tokens, and LLaMA3-8B [15]. In this setup, the register tokens act as “fixed outlier sinks” [11], effectively forming a closed-set vocabulary for outlier attraction, analogous to the tokenization setup in LLMs. As shown in Fig. 9, when ViTs are equipped with four learned register tokens, they begin to exhibit outliers in early layers (i.e., 2nd layer), mirroring the behavior observed in LLMs. This supports our hypothesis that continuous tokenization in ViTs plays a crucial role in the emergence of outliers in the intermediate layers.

N. Weight-only Quantization

We demonstrate the effectiveness of RegCache when combined with weight-centric methods, i.e., weight-only quantization, which are commonly used in LLMs to reduce memory usage and deployment cost. Specifically, we adopt AWQ [29], a widely used weight-only quantization method, as the baseline, using a group size of 128 and bitwidths of 8, 6, 4, and 3. Across all configurations, RegCache consistently improves performance over vanilla AWQ, demonstrating its complementary benefits even in memory-constrained quantization settings. However, as noted in Sec. 1, unlike autoregressive LLMs, vision encoders are typically compute-bound, making weight-only quantization less effective.

Table 16. Zero-shot image classification accuracy (%) under weight-only quantization (AWQ).

Model	FP32	Method	Weight-only (AWQ) Bits			
			W3A16	W4A16	W6A16	W8A16
CLIP-B/16	68.32	AWQ	62.08	66.73	67.80	68.05
		+ RegCache	63.08 (+1.00)	67.06 (+0.33)	67.94 (+0.14)	68.14 (+0.09)

O. With Hadamard Rotation Quantization

Motivated by recent works in the LLM literature on utilizing Hadamard rotations for outlier mitigation [1, 36], we have also explored whether RegCache can also be combined with such methods. In particular, we follow the adaptations of ViDiT-Q [58] to apply Hadamard rotations to all linear layers in the transformer blocks.⁷ As reported in Tab. 17, RegCache improves accuracy in most settings when used as a plug-in method, indicating that suppressing extreme outliers in the rotated domain can further enhance quantization performance.

Table 17. Zero-shot image classification accuracy (%) on top of QuaRot [1]

Method	CLIP		OpenCLIP	
	W6A6	W8A8	W6A6	W8A8
FP32	68.32		70.22	
Naïve	0.17	34.01	0.47	46.12
QuaRot	55.86	66.38	59.49	68.50
QuaRot + RegCache	56.05	66.84	59.76	68.50

⁷There is one exception: we do not use the Walsh–Hadamard matrix for the value and output projection matrices, as in the ViDiT-Q implementation. Also, we have empirically observed that naively applying QuaRot to vision encoders tends to severely damage the model performance.

P. Combining with LLM Outlier-mitigation Methods

We evaluate whether SmoothQuant (SQ)—a widely used outlier-mitigation PTQ technique for LLMs—transfers to ViT-based vision encoders. As shown in Tab. 18, SQ alone yields only marginal improvements over the naïve quantization baseline, consistent with prior observations on ViTs [47]. While RegCache provides clear additional gains when applied on top of SQ, we further note that ViT-specific outlier mitigation methods such as RepQ-ViT (RepQ) may be a more effective direction for vision encoders.

Table 18. **W8A8 quantization on vision encoders.** Zero-shot ImageNet-1k accuracy (%) under W8A8 activation quantization.

	FP32	Naïve	LLM PTQ method		ViT PTQ method	
			SQ	SQ + ours	RepQ	RepQ + ours
CLIP	68.32	34.01	35.54	60.30 (+24.76)	67.39	68.10 (+0.71)
OpenCLIP	70.22	46.12	46.50	67.07 (+20.57)	68.70	70.06 (+1.36)
SigLIP	76.05	69.71	70.55	74.65 (+4.10)	75.23	75.94 (+0.71)
SigLIP2	78.47	26.04	28.20	72.45 (+44.25)	76.43	77.13 (+0.70)